Validating city-scale surface water flood modelling using crowd-sourced data

2016 Environ. Res. Lett. 11 124011

(http://iopscience.iop.org/1748-9326/11/12/124011)

Environmental Research Letters

LETTER

Validating city-scale surface water flood modelling using crowd-sourced data

Dapeng Yu[1], **Jie Yin**[2,3] **and Min Liu**[2,3]

[1] Centre for Hydrological and Ecosystem Science, Department of Geography, Loughborough University, UK
[2] Key Laboratory of Geographic Information Science (Ministry of Education), East China Normal University, People's Republic of China
[3] School of Geographic Sciences, East China Normal University, People's Republic of China

E-mail: rjay9@126.com

Keywords: surface water flooding, storm sewer modelling, urban flooding, FloodMap, Shanghai

OPEN ACCESS

RECEIVED
5 May 2016

REVISED
15 November 2016

ACCEPTED FOR PUBLICATION
16 November 2016

PUBLISHED
30 November 2016

Abstract

Surface water and surface water related flood modelling at the city-scale is challenging due to a range of factors including the availability of subsurface data and difficulty in deriving runoff inputs and surcharge for individual storm sewer inlets. Most of the research undertaken so far has been focusing on local-scale predictions of sewer surcharge induced surface flooding, using a 1D/1D or 1D/2D coupled storm sewer and surface flow model. In this study, we describe the application of an urban hydro-inundation model (FloodMap-HydroInundation2D) to simulate surface water related flooding arising from extreme precipitation at the city-scale. This approach was applied to model an extreme storm event that occurred on 12 August 2011 in the city of Shanghai, China, and the model predictions were compared with a 'crowd-sourced' dataset of flood incidents. The results suggest that the model is able to capture the broad patterns of inundated areas at the city-scale. Temporal evaluation also demonstrates a good level of agreement between the reported and predicted flood timing. Due to the mild terrain of the city, the worst-hit areas are predicted to be topographic lows. The spatio-temporal accuracy of the precipitation and micro-topography are the two critical factors that affect the prediction accuracies. Future studies could be directed towards making more accurate and robust predictions of water depth and velocity using higher quality topographic, precipitation and drainage capacity information.

1. Introduction

Surface water flooding occurs when precipitation overwhelms the drainage system and the excess water cannot be drained away. It is increasingly perceived to be a widespread and frequently occurring type of natural hazard in many regions around the world, and possibly a manifestation of the intensified precipitation cycle due to climate change and variability. It proves especially problematic for developing and emerging countries, where the capacity of the existing storm sewer systems is often either myopically designed in the first place or outpaced by the magnitude of increased runoff associated with urbanization. Indeed, surface water flooding may also pose widespread problems for developed countries with well-established sewer systems. For example, the majority of the 2007 floods in the UK originated from overloaded storm sewers in developed areas, and among the buildings affected, around 25% were constructed during the previous 25 years (Pitt 2008). Although often associated with shallow water depth compared with fluvial and coastal flooding, the impact can be equally far-reaching and widespread. Apart from inundating properties, traffic disruption and its indirect consequences such as loss of productivity and business opportunities are the foremost impacts a surface water flood event can exert in urban environments.

The advent of computational methods for simulating both subsurface pipe flow within the urban storm sewer system and surface runoff has enabled the numerical modelling of surface water flooding in recent decades (e.g. Hsu *et al* 2000, Dong and Lu 2008). Various modelling approaches to surface water flooding exist, including: (i) coupling a 1D

storm sewer model with a 1D surface flow model (Mark *et al* 2004, Maksimović *et al* 2009); (ii) representing storm sewer flow routing in 1D and surface flow in 2D (e.g. Hsu *et al* 2000, Schmitt *et al* 2004); and (iii) considering only 2D surface flow routing but neglect or simplify the representation of the surface & sewer flow interaction (e.g. Fewtrell *et al* 2011, Sampson *et al* 2013). Accordingly, these three types of models are termed as '1D/1D', '1D/2D' and '2D' respectively in literature, with the first two often collectively referred to as 'dual drainage modelling' defined by Djordjević *et al* (1991). A brief review of the dual drainage modelling concept and its implementation is provided by Schmitt *et al* (2004). Key studies related to this concept are further elaborated by Smith (2006), along with a discussion on the role of GIS in providing model flow and topographic inputs.

Whilst computationally efficient, the key limitation of the '1D/1D' approach is its representation of the surface flow routing, which may be oversimplified in situations where water is no longer confined within streets and lateral spreading of flood water occurs. In contrast, the '1D/2D' approach represents surface flow in a more intuitive way and it considers surface flow routing in two dimensions. This approach has been implemented in both the street(s) level (e.g. Schmitt *et al* 2004, Leandro *et al* 2009, Seyoum *et al* 2012) and at the city scale (e.g. downtown Taipei, 140 km^2, Hsu *et al* 2000), using either a loosely-coupled approach where the 1D and 2D models run in sequence (e.g. Hsu *et al* 2000, Seyoum *et al* 2012) or a tightly-coupled approach where the 1D and 2D models are solved simultaneously (e.g. Schmitt *et al* 2004, Leandro *et al* 2009). The tightly-coupled approach is hydraulically robust as the interaction between the sewer and surface flow is fully accounted for in two directions. However, the loosely-coupled approach treats surcharge of the 1D model as non-returnable flow on the surface due to its sequential treatment of the sewer/surface interaction as mass gain and loss to the 1D/2D models. In both methods, flooding caused directly by surface runoff is not considered but treated as inputs to the storm sewer model. Surcharge from the storm sewer manholes is the only source of surface flood. In addition, although it can be rightfully regarded as the state of art in the current modelling of surface water flooding at the local scale, in many developing nations, the practical implementation of the dual drainage concept is challenging due to a number of reasons, including: (i) the reliance on GIS preprocessing to obtain overland flow pathways and ponds; (ii) the (un)availability of storm sewer system profiles, especially at the city scale; (iii) the complexity and uncertainty of deriving hydrologic inputs to the 1D sewer model in an urban environment; and (iv) the lack of topographic data with adequate quality to represent urban features. More recently, 2D surface flow routing techniques have been used to simulate the surface runoff originating from point sources (e.g. manholes) with synthetic or model-derived flow hydrographs (e.g. Mignot *et al* 2006, Fewtrell *et al* 2011, Sampson *et al* 2013). In this approach, the interaction between surface runoff and storm sewers is considered as insignificant, with sewer surcharge as the main source of surface water flooding.

One important area of research in surface water flood modelling is the representation of the surface runoff directly resulting from heavy precipitation at the local scale. Aronica and Lanza (2005) found that micro-topography may produce local flooding with significant water depth and velocity in zones of flow concentration. The dual drainage approach calculates the lump-sum of the precipitation-induced direct surface runoff as an input to the storm sewer model (e.g. using the rational approach; Hamill 2010), assuming: (i) no significant direct surface runoff occurs and water accumulates only to storm drains; (ii) storm sewer inlets are capable of collecting the entire runoff (e.g. Leandro *et al* 2009); and (iii) storm sewer surcharge (e.g. at manholes) is the sole source of surface runoff. However, in some situations, localized direct surface runoff immediately following the precipitation can be far more significant than sewer surcharge, especially during extreme precipitation events such as short-duration high-intensity tropical cyclones/typhoons/hurricanes. Urban storm sewer systems may not take in all the surface runoff during extreme events and direct surface runoff can overpass manholes and accumulate to form ponding in topographic depressions due to inlet efficiency (Aronica and Lanza 2005). Sampson *et al* (2013) modelled surface water flood at a local scale (0.5 km^2) with a uniform rainfall input followed by a synthetic culvert surcharge using a flood inundation model (LISFLOOD-FP). This study focused on: (i) developing methods for routing rainwater from elevated features; and (ii) comparing with commercial modelling packages to evaluate model performance. Hydrological factors (e.g. infiltration and evapotranspiration) are not considered and there were no observation data available for model validation. Yu and Coulthard (2015) improved on this and described the development of a surface water flood inundation model (FloodMap-HydroInundation) applied with relatively high resolution (10 m and 20 m) to the City of Hull and evaluated the importance of catchment-scale hydrological parameters for urban surface water flood modelling. Yin *et al* (2016a) applied the model with a street-level resolution of 2 m to the inner-city area of Shanghai and focused on the impact of land subsidence over decadal timescale on surface water flood risks in the city. The modelling results were compared with point-based depth gauging records. Furthermore, the impact of urban surface water flood risks on road transport disruption was evaluated in the intra city of Shanghai by Yin *et al* (2016b). These studies demonstrate the capacity of the model for fine resolution street-level scale modelling

of surface water flood risks at the local scale (e.g. district).

At the city-scale, a recent study (Hénonin *et al* 2013) simulates the July 2012 event that occurred in Beijing, focusing on the use of multi-grid approaches in a 2D commercial model (MIKE 21, DHI 2010) whereby a sub-grid finer mesh is nested within a coarser one (Yu and Lane 2006b, 2011). Due to data constrain, simulations were undertaken at selected five sites rather than the whole city (1000 km^2), with areas ranging from 8.3 to 44.9 km^2. Rainfall was applied as direct boundary condition and hydrological processes were not considered. Drainage capacity was applied as a constant evaporation rate to the 2D model. The multi-grid approach was found to produce more detailed and realistic predictions at the local scale with good computational efficiency. An earlier study by St Domingo *et al* (2010) coupled a hydrological model (MIKE SHE) with a hydraulic model (MIKE Flood) for catchment scale flood inundation modelling and the coupled model was applied to a small catchment (6 km^2). This provides a useful addition to the modelling methods currently used for urban surface water flood modelling, in particular for places where land hydrology and surface runoff affect directly surface water flooding in urban environment.

This study builds on the model development in Yu and Coulthard (2015) and describes: (i) the application of the simplified modelling approach to identify areas vulnerable to surface water flooding risks during extreme precipitation events at the whole city-scale; and (ii) the use of a unique crowd-sourced dataset for model validation. Direct surface runoff is assumed to be the primary source of surface flow during extreme precipitation events. Rather than detailed flow routing, the focus of the model is to derive, at the city-scale, areas potentially at risks to surface flooding during extreme precipitation events, considering the spatio-temporal heterogeneity of precipitation, drainage capacity and land use in the urban landscape. This approach complements the existing approaches to the evaluation of surface water flooding which typically focus on sewer surcharge induced surface flooding at localised locations.

2. Model description

The model (FloodMap-HydroInundation2D) was developed based on the modified version (inertial-based) of FloodMap (Yu and Lane 2006a), and integrates surface flow routing processes with key hydrological processes during an urban storm event, including infiltration and evapotranspiration. The model development has been described in Yu and Coulthard (2015). Here we reproduce the main structure of the surface flow routing and the way infiltration and evapotranspiration are represented.

2.1. Surface runoff

The 2D inundation model takes the same structure as the inertial model of Bates *et al* (2010), but with a different approach to calculate time step. If we neglect the convective acceleration term in the Saint-Venant equation, the momentum equation for flow along the x-axis becomes:

$$\frac{\partial q}{\partial t} + \frac{gh\partial(h+z)}{\partial x} + \frac{gn^2q^2}{R^{4/3}h} = 0 \quad (1)$$

Where q is the flow per unit width, g is the acceleration due to gravity, R is the hydraulic radius, z is the bed elevation, h is the water depth and n is the Manning's roughness coefficient. A similar formulation can be written for flow along the y-axis. Discretizing the equation with respect to time produces:

$$\frac{q_{t+\Delta t} - q_t}{\Delta t} + \frac{gh_t\partial(h+z)}{\partial x} + \frac{gn^2q_t^2}{h_t^{7/3}} = 0 \quad (2)$$

To further improve this, one of the q_t in the friction term can be replaced by $q_{t+\Delta t}$ and this gives the explicit expression of the flow at the next time step:

$$q_{t+\Delta t} = \frac{q_t - gh_t\Delta t\left(\frac{\partial(h_t+z)}{\partial x}\right)}{(1 + gh_t\Delta tn^2q_t/h_t^{10/3})} \quad (3)$$

The flow in the x and y directions is decoupled and take the same form. Discharge is calculated at the cell edges and depth at the cell centre. In order to maintain model stability and minimize numerical diffusion, the Forward Courant–Freidrich–Levy Condition (FCFL) approach described in Yu and Lane (2011) for the diffusion-based version of FloodMap is used in the inertial model to calculate time step:

$$\Delta t <= \min\left(\frac{wd_id_jn}{d_i^{1.67}(S_i)^{1/2} + d_j^{1.67}(S_j)^{1/2}}\right) \quad (4)$$

where w is the cell size, d_i and d_j are the effective water depths, S_i and S_j are water surface slopes, and i and j are the indices for the flow direction in the x and y directions, respectively.

2.2. Infiltration and evapotranspiration

Infiltration over saturation is represented with the widely used Green–Ampt infiltration equation to model infiltration to soil. It takes the following form:

$$f(t) = K_s\left(\frac{\varphi_f + h_o}{z_f} + 1\right) \quad (5)$$

Where K_s is the hydraulic conductivity of the soil at field saturation, φ_f is the capillary potential across the wetting front, h_o is the ponding water on the soil surface, and z_f is cumulative depth of infiltration. Therefore the rate of infiltration approximated by the Green–Ampt equation is a function of the capillary potential, porosity, hydraulic conductivity and time. Hydraulic conductivity is used as a calibration parameter in this study. The value of capillary potential is kept at a constant of 0.73 meters.

Evapotranspiration is approximated using a simple seasonal sine curve for daily potential evapotranspiration (Calder *et al* 1983) with the equation below:

$$E_p = \overline{E_p}\left[1 + \sin\left(\frac{360i}{365} - 90\right)\right] \quad (6)$$

Where $\overline{E_p}$ is the mean daily potential evapotranspiration and i is the day of the year.

2.3. Drainage capacity

Another source of mass loss for urban storm water runoff is the storm sewer system through which storm water can be drained naturally or pumped. Drainage capacity is represented by the unit-time amount of surface-accumulated water (surface flow and rainfall) that can be collected by the storm sewer system, usually expressed as mm per hour and corresponding to a certain return period of rainfall. For each time step, the amount of flow loss to the urban storm sewer systems can then be calculated by scaling the design drainage capacity (mm/hour) for the time step. It should be noted that the sewer hydraulic processes and their effects on the inundation were not explicitly represented by this model. Rather, the model captures the mass loss to storm sewer system based on its design capacity. The model is particularly suited for applications in large-scale metropolitan area where the numerical modelling of city-wide sewer system hydrodynamics is challenging due to the volumes of data required at the city scale which typically involves millions of manholes and drains.

In distributed models like the one presented herein, whether surface flow will occur at a particular dry pixel therefore depends on the rainfall intensity at the point. When a pixel is wet already, if the total existing water depth plus the rainfall depth for a particular time step is less than the drainage capacity (scaled for the time step), no surface runoff will occur and vice versus depending on local topography. The capacity itself does not vary over time and is directly related to the design standard of the storm sewer system (design drainage capacity).

In the model, we assume that storm sewer system drains water away at the maximum design drainage capacity and no loss of capacity due to surcharge is considered. However, the value can also be scaled to represent the effect of blockage by debris or malfunction of the storm sewer system including pumping stations. Moreover, at the city scale, drainage capacity is rarely uniform. Therefore, the model allows distributed drainage capacity to be incorporated on a cell by cell basis.

3. Model applications: case study and data availability

3.1. Study site

One of the surface water flooding hotspots in recent years is the South and Southeast Asia, where surface water flooding events, typically associated with typhoon, are frequently recorded. China in particular is one of the worst hit regions. The most devastating surface water flood event in recent years occurred in Beijing on 21 July 2012, during which 79 causalities were reported. Although this is widely seen as an extremely rare event, the lack of preparation (both infrastructural and societal) to extreme flood events are noted by many (Chin 2012, Xu 2012). Across the south and southeast China, many cities appear to be facing more surface water flooding in recent years amongst the occurrence of more frequent high-intensity precipitation events (Zhai *et al* 2005), coincide with the rapid urban expansion which results in decreased surface permeability and increased runoff. The risk is further compounded by the perceived impact of climate change and variability, which is predicted by IPCC (2007) to result in an intensified precipitation cycle.

The model was tested in the city of Shanghai, China, a coastal megacity developed on the Yangtze River Delta and Huangpu River floodplain (6340 km^2, figure 1). Its topography is characterized by a mild sloped terrain. Notably, in the central districts, the ground elevation is mostly less than 3.0 m, and the lowest elevation is around 2.3 m. Surface water flooding events are frequent in Shanghai and they are typically associated with typhoons which occur multiple times on an annual basis. Shanghai has a modern storm sewer system. The drainage capacity of the storm sewer system is 36 mm h^{-1} in most urban areas and 27 mm h^{-1} in relatively rural areas, equivalent to a 1 in 1 year and 1 in half year design standard. Only in a very limited few places the design standard is 54 mm h^{-1}. As a result, surface water flooding is expected each year, demonstrated by an archive of events since 1997 compiled by Wu *et al* (2012). With the average tidal level during the flood season ranging between 4.0 m and 4.35 m, the fastest rising sea level in China (Yin *et al* 2013a, 2013b) and an alarming land subsidence rate (nearly 2 meters in total between 1921 and 2007, and stabilized at 5 mm/year since 2010 due to groundwater recharge), the risk of flooding from surface water source appears to be increasing in recent decades based on rainfall and event analysis (Wu *et al* 2012). Despite the large-scale construction of urban storm sewer systems, the problem of surface water flooding still persists (Wu *et al* 2012) and between 1980 and 1993, there were on average 251 road sections and 52 700 buildings suffering from waterlogging every year (Yuan 1999). Traffic disruption and property damages are frequently reported by the public.

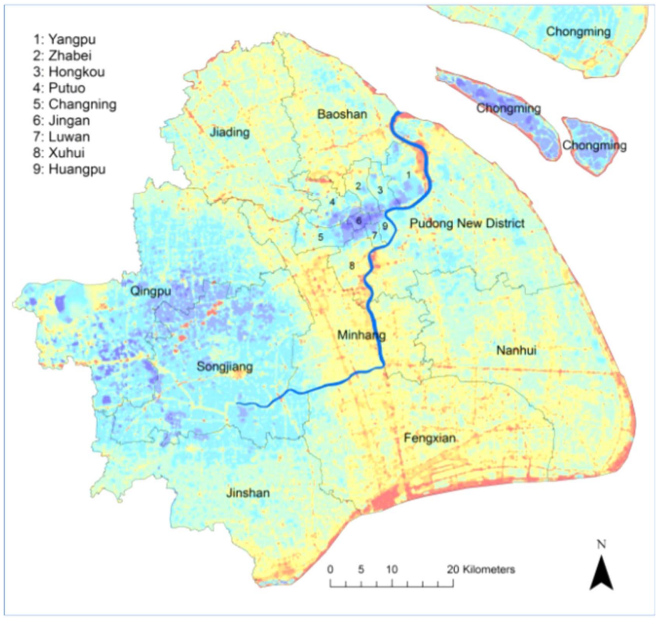

Figure 1. Administrative districts overlain with the DEM of Shanghai. Numbered districts are the inner-city districts.

The surface water flood event modelled is storm-induced and occurred on the 12 August 2011, during which a total of 86 mm rain was recorded in the Huangpu Park gauging station at the city centre within 6 h (6 am to 12 am), causing considerable traffic disruption in the morning rush hours and flooded properties.

3.2. Data availability and processing

3.2.1. Topographic data

The topographic data available at the city-scale in Shanghai is a 0.5 m contour line. This is processed to a 50 m Digital Elevation Model to represent the city's topography. In total, 3.7 million cells are used, representing the top limit of the computational resources available. Roughness is represented by floodplain Manning's n in the model for individual pixels, where urban area, farmland, grasses, water bodies and bareland are assigned a value of 0.01, 0.05, 0.06, 0.03 and 0.035, respectively.

3.2.2. Precipitation data

The precipitation inputs to distributed rainfall runoff models are typically derived based on: (i) a single rainfall gauging station if the catchment is sufficiently small or data is limited; or (ii) interpolation of a number of gauging station records if the catchment is relatively large and the gauging network is of sufficient density. Given the uncertainty usually associated with gauging records and the spatial variation of rainfall, interpolation of distributed rainfall gauging records is often considered to be a more reliable approach to represent rainfall spatial and temporal variation. For Shanghai, the spatial and temporal resolution of the rainfall gauging network (44 rain gauges recording at a 15 min interval) enabled the time series of distributed rainfall to be derived. Precipitation rate was calculated based on the kriging interpolation of the tipping bucket measurements and used as rainfall inputs to the model. It should be note that the spatial pattern (local higher intensities) may be controlled by one single rain gauge for some locations. Generally, radar rainfall data such as Quantitative Precipitation Estimation (QPE) can be used to improve interpolation accuracy (Ochoa-Rodriguez *et al* 2015, Wang *et al* 2015), but it is not available in the Shanghai. The time series of rainfall distribution interpolated from the gauging stations are shown in figure 2. Rainfall occurred first to the west of the city and then the storm centre moved to the inner city. It persisted over the city centre from around the 2nd hour (8 am) and deposited a large amount of rainfall in the inner city districts (figure 2). The rainfall hyetographs of the two stations (Huangpu Park and Jiangsu Road) with the highest amount of recorded rainfall are shown in figure 2(b). The total amount of rainfall in the Huangpu Park station is around 80 mm, equivalent to a return period of 30–50 years based on historical data analysis.

3.2.3. Observed inundation

Observation data for the event simulated exists in two forms, including: (i) point measurements of water depth with digital meters, operated by the Shanghai Municipal Water Affairs Bureau and typically installed underneath highway overpasses; and (ii) reported localized flood incidents at the street or house level by the public ('crowd source') and collated through a web-based emergency incident reporting portal, operated by the government and accessible to the public. Here we refer a flood incident as a logged report of an

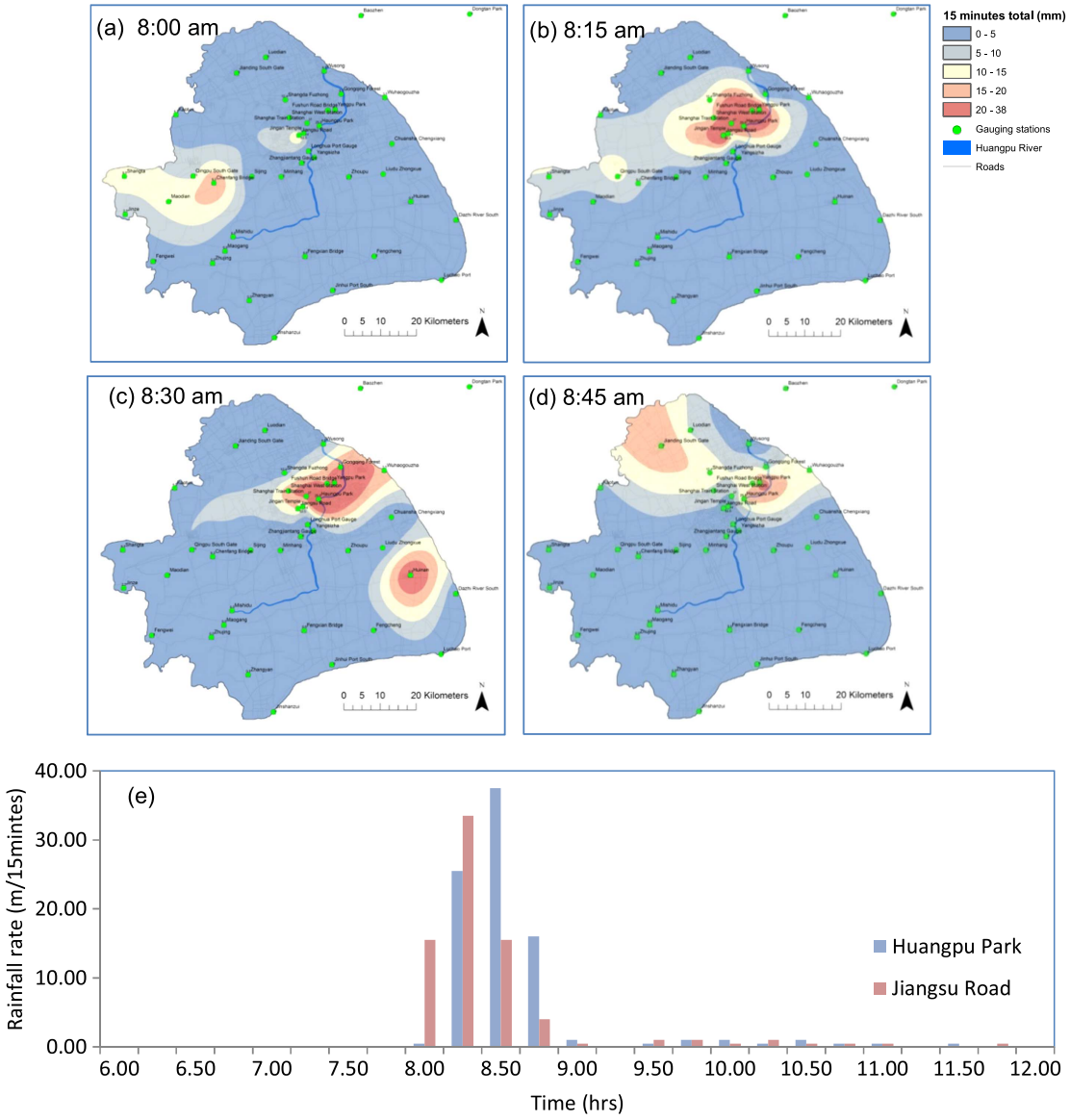

Figure 2. (a)–(d): spatial and temporal distribution of peak precipitation during the August 2011 storm event occurred in Shanghai; (e) rainfall time series at the two gauging stations with the highest rainfall amount.

event by the web portal whereby the reporter is affected directly by surface water flooding. The monitoring points are the hotspots of surface water flooding in Shanghai and strategically installed to assess the impact of surface water flooding on traffic disruption. The exact locations of the monitoring points are not available due to various restrictions. However, the roads where the monitoring points are located have been obtained. This is shown in figure 3. Flood incidents reported by the public can be extensive and this usually contains the exact location of the property/road affected, a description of its nature and, in some cases, an estimate of the depth. However, given the predictive focus of the model, and the resolution & accuracy of the input data, including the DTMs and rainfall distribution, model validation using water depth is not considered in this application. Rather, we focus on evaluating the general agreement between the model predicted risky areas with both the hotspots monitored and the 'crowd sourced' flooded locations, i.e. a Boolean comparison of whether a reported/monitored flooded site is predicted as flooded. For the event considered, 490 localized flooding incidents were reported through the information portal. After removing the duplicate records and records that are not related to surface water flooding, 298 records are retained and 250 points are located in the inner city districts. The locations of the points where incidents are reported are determined using the Google Map service and geo-referenced in GIS. The point locations are shown in figure 3, along with the roads monitored by the Shanghai Municipal Water Affairs Bureau.

3.3. Specification of drainage capacity

Distributed drainage capacity is used in the model to represent its spatial variability. This is specified according to the design capacity of the storm sewer

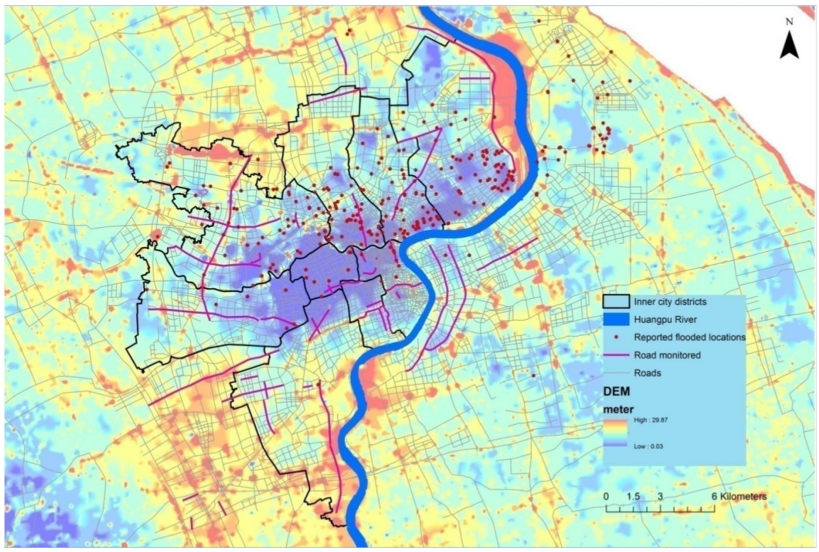

Figure 3. Roads where digital meters are installed by the government, and locations where local flood incidents were reported by the public during the 12 August 2011 event.

system of 36 mm h^{-1} in most urban areas and 27 mm h^{-1} in relatively rural areas, and 54 mm h^{-1} in isolated areas. Due to the mild terrain of the city, Shanghai is largely drained by pumping stations rather than natural drainage through gravity, discharging pumped water directly to the river channels. Therefore, the sewer hydraulic processes do not obviously influence the surface inundation in Shanghai in most cases and surface water flooding arises dominantly from surface water runoff. When high tides occur, the natural drainage is even more restricted and the city can only be drained through pumping stations. In the simulations undertaken, it is assumed that the storm sewer system functioned fully during the flood event simulated and there is no evidence suggesting otherwise.

3.4. Model calibration and sensitivity analysis

3.4.1. Sensitivity to mesh resolution and roughness parameterisation

It is recognized that a finer mesh would better represent the topographic peculiarities and the presence of discontinuities on urban topography. Given the size of the study area, if a 50 m DEM is used to represent the topography, 3.7 million pixels are required. This represents the top limit of the number of pixels a high-performance desktop workstation can handle for 2D modelling. A finer mesh is therefore computationally infeasible for the whole site for sensitivity analysis to mesh resolution. To evaluate the model sensitivity to mesh resolution, we choose the inner city area (the 9 districts shown in figure 1) where DEMs of 20 m, 30 m, 40 m and 50 m are used. Sensitivity analysis was also undertaken to evaluate the model response to variation of hydraulic roughness. A uniform roughness value (n) ranging from 0.01 to 0.1 with a 0.01 interval was used in the analysis. In conjunction with mesh resolutions (20 m, 30 m, 40 m and 50 m), 40 simulations were undertaken and the results are presented in section 4.1.

3.4.2. Model calibration with hydraulic conductivity

Model calibration was undertaken to evaluate the sensitivity of model prediction to infiltration, represented by the hydraulic conductivity (K_s) parameter. It should be recognized that determining soil hydraulic conductivity is highly complex. Studies determining the soil hydraulic conductivity values have either used empirically-based correlation methods or through *in situ* hydraulic laboratory measurements. The latter is infeasible for urban catchments due to practical constrains. We use the correlation methods to estimate soil hydraulic conductivity for Shanghai. Such methods typically associate K_s with soil properties (i.e. texture, pore-size and grain size distribution) or soil mapping units (Oosterbaan and Nijland 1994). However, such methods can be highly uncertain due to the simplified and generalized nature of empirical derivations. The dominate type of soil texture in Shanghai is silt loam, consisting of poorly drained soils that formed in alluvium from mixed sources. The K_s value for the study site is therefore determined based on the lower range of the typical K_s suggested by Smedema and Rycroft (1983) and through a calibration process, during which the percentage of reported incidents falling within the flood area is used as a criterion. The values of saturated hydraulic conductivity are varied between 1 to 10 mm h^{-1}, with a regular interval of 1 mm h^{-1}. This captures the range of infiltration values associated with the soil type in Shanghai, covering the lower range of the K_s values suggested by Smedema and Rycroft (1983), and reflecting the urbanized nature of the study area.

3.4.3. Evaluation metrics

For both sensitivity analysis and model calibration, three standard metrics typically used in flood modelling (e.g. Bates and De Roo 2000, Yu and Lane 2011) are used to evaluate the model response, including the total inundation area, Fit statistics (F) and Root Mean Standard Error (RMSE). These are calculated over time for a certain interval (5 min in this study for the 6 h event), with the F and RMSE calculated against a reference simulation. The F statistic is commonly used for evaluating the goodness of agreement between predicted inundation extent and the reference (Bates and De Roo 2000, Horritt and Bates 2001). It can be defined as follow:

$$F = \frac{A_o}{A_r + A_s - A_o}$$

where A_r is the referenced wet areas, A_s is the predicted wet areas, and A_o is the overlap of A_r and A_s. F varies between 1 for a perfect fit and 0 when no overlap exists.

The RMSE is a useful metric for the comparison of water levels (or depths) between predicted and observed/referenced water depths, on a cell by cell (point to point) basis in the case of flood inundation modelling. The metric is calculated by:

$$\mathrm{RMSE} = \sqrt{\frac{\sum_{i=0}^{n}(d_i^s - d_i^r)^2}{n}}$$

where d_i^s and d_i^r are the predicted and referenced water levels (or depths) respectively, i is the index of the wet cells and n is the total number of wet cells in the prediction and observation.

4. Results

4.1. Sensitivity to mesh resolution and roughness parameterisation

Figure 4 plots the three evaluation metrics used in this study to illustrate the model sensitivity to mesh resolution and roughness specification over time, including the total inundation area (figure 4(a)), Fit statistic (figure 4(b)) and Root Mean Standard Error (RMSE) (figure 4(c)), grouped according to the roughness value for each mesh resolution.

Table 1 compares, for each roughness value, the percentage difference in peak inundation area between the 30 m, 40 m and 50 m with the reference simulation of 20 m, therefore an evaluation of model sensitivity to mesh resolution.

To demonstrate the sensitivity to roughness specification for a specific mesh resolution, table 2 calculates the percentage of difference in peak inundation area between a reference simulation with an n value of 0.01 and the simulations with other n values specified in section 3.4.1.

Evaluation of: (i) the agreement between the inundation extents (F, figure 4(a)); and (ii) the variation between water depths (RMSE, figure 4(b)) is presented in tables 3 and 4 respectively for the maximum F and RMSE values obtained from each simulation.

The difference between the predicted maximum water depths of the 50 m simulation is compared with the 20 m, 30 m and 40 m to demonstrate the spatial distribution of depth sensitivity in figure 5.

Figure 6 demonstrates the spatial sensitivity of the model response to roughness parameter. The difference between the maximum water depth predicted by simulations with $n = 0.1$ and $n = 0.01$ is calculated on a cell by cell basis, demonstrating the spatial variation of depth prediction.

4.2. Sensitivity to hydraulic conductivity

Figure 7 shows the water depth difference between simulations with various hydraulic conductivity values and the default simulation with a hydraulic conductivity of 0.001 m h^{-1}. As expected, the depth difference increases proportionately with the extent of K_s deviation from the default value of 0.001 m h^{-1}. There are large areas with depth difference greater than 2 cm and in some cases the difference exceeds 10 cm. Figure 9 shows the statistical analysis of agreement between water depth and extent over time. Over the whole simulation domain, global measurement of depth difference Root Mean Standard Error (RMSE) (figure 9(b)) suggests that, the model is insensitive to K_s when the overall water depth is considered. However figure 8 shows that the difference can be localized in topographic lows. This is confirmed by figures 8(a) and (c) where both the total inundated area and the spatial agreement between the predicted extents vary to a large extent. For all simulations, over 90% of the observed points in the inner city districts fall within the predicted flooded area, with the highest percentage (93%) associated with the reference K_s value of 0.001 m h^{-1}. This is therefore used in the subsequent analysis.

4.3. Time series of flooded areas

The predicted water depths across the city at discrete time periods are plotted in figure 9. These demonstrate the spatial and temporal evolution of surface water flooding during the course of the storm event. Given the mild terrain, surface flooding is locally originated and synchronized with the timing and spatial distribution of rainfall. Extensive surface water flooding occurs in the city centre from around the 8:30 am, albeit mostly with shallow water depth of less than 5 cm. Shortly after the peak of the precipitation (~9:00 am), predicted surface flooding reaches its maximum extent (figure 10) and magnitude (figure 9). Afterwards, flood starts to recede, through infiltration, evapotranspiration and storm sewer network.

4.4. Maximum depth and extent predicted

The maximum water depth during the course of the flood event is shown in figure 11(a) for the whole city

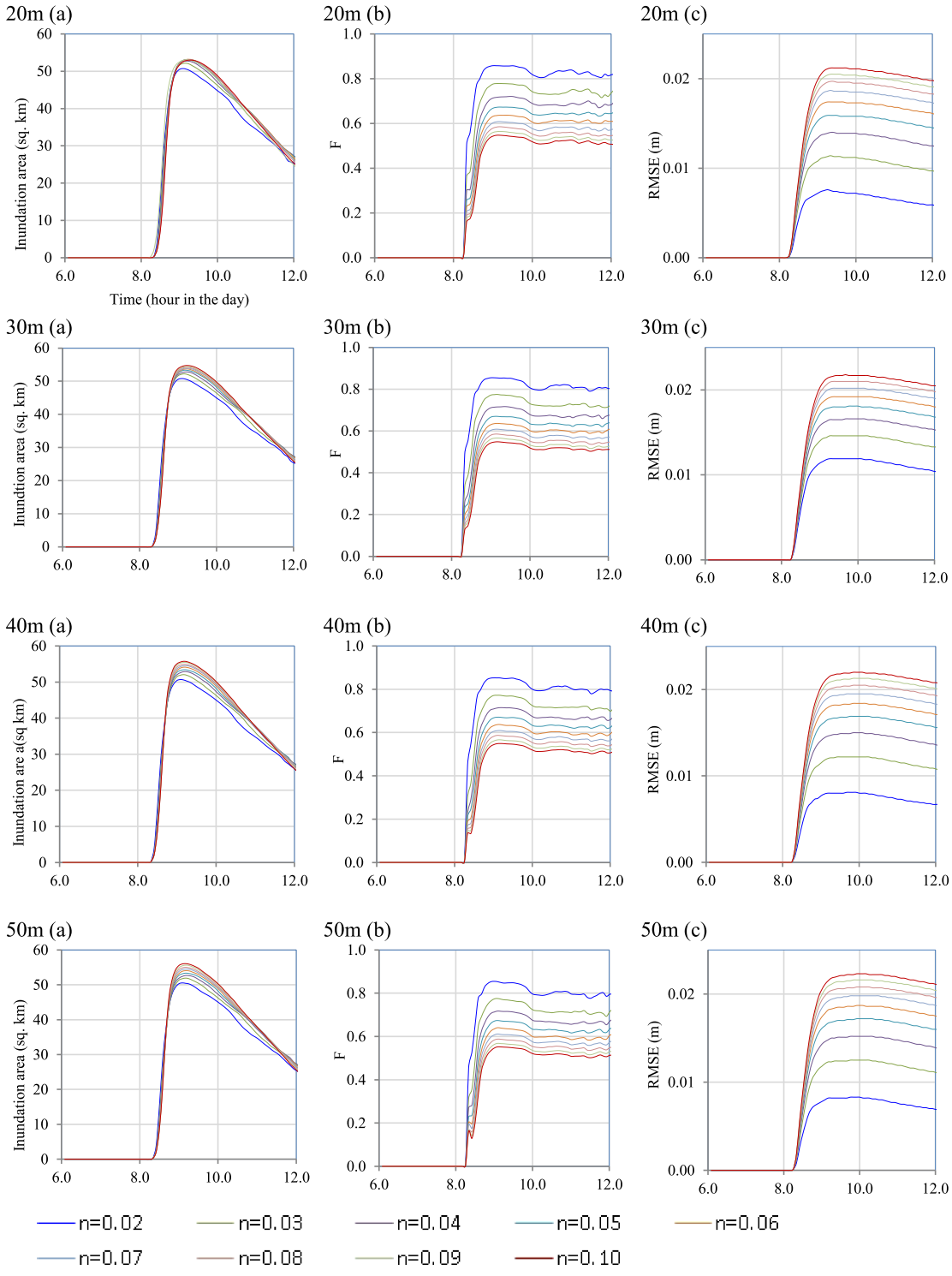

Figure 4. Sensitivity analysis of the model to mesh resolution and roughness parameterisation (at the inner-city scale).

and figure 11(b) for the inner city districts. We use 2 cm as the threshold for surface water flooding and treat water shallower than 2 cm as sheet flow which takes the form a thin film running continuously on the surface and not concentrate to form channels or accumulate in topographic lows. Results show that extensive surface water flooding is predicted, both in the inner city district to the west of the Huangpu River and the newly-developed Pudong New District to the east. Apart from the inner city districts, Jiading, Qingpu and Nanhui districts are also predicted to have suffered from surface water flooding during the event. In most of the flooded places, water depths are between 2 cm and 15 cm (71%). Areas with depth between 15 cm to 30 cm account for 28% of the total flooded areas. Some of the areas are inundated with water depth above 30 cm (0.3%) and in some topographic depressions, water depth reaches more than 50 cm (0.01%).

Table 1. Percentage difference between the peak inundated areas associated with different mesh resolutions (m.r.), compared for each roughness value. For each roughness value, m.r. = 20 m is used as the reference simulation and the difference is calculated therefrom.

Difference in peak inundation (%) (ref. is m.r. = 20 m)	$n = 0.01$	$n = 0.02$	$n = 0.03$	$n = 0.04$	$n = 0.05$	$n = 0.06$	$n = 0.07$	$n = 0.08$	$n = 0.09$	$n = 0.10$
30 m	−0.2	0.2	0.2	0.2	0.4	1.0	1.4	2.0	2.6	3.3
40 m	−0.4	−0.1	−0.2	0.3	0.5	1.7	2.5	3.3	4.5	5.2
50 m	−0.7	−0.3	−0.4	−0.1	0.4	1.6	2.6	3.6	4.8	5.8

Table 2. Percentage difference between the peak inundated areas associated with different roughness values for each mesh resolution. For each mesh resolution, $n = 0.01$ is used as the reference simulation and the difference is calculated therefrom.

Difference in peak inundation (%) (ref. is $n = 0.01$)	$n = 0.02$	$n = 0.03$	$n = 0.04$	$n = 0.05$	$n = 0.06$	$n = 0.07$	$n = 0.08$	$n = 0.09$	$n = 0.10$
20 m	1.8	4.5	5.5	6.2	6.3	6.3	6.2	6.1	6.0
30 m	2.1	4.8	5.9	6.8	7.4	7.8	8.3	8.7	9.2
40 m	2.1	4.7	6.2	7.1	8.3	9.0	9.7	10.5	11.0
50 m	2.1	4.7	6.1	7.2	8.4	9.2	10.1	11.0	11.7

Table 3. F statistics calculated for different roughness values in each mesh resolution. The simulation with $n = 0.01$ for each resolution is used as the reference simulation.

F (%)	$n = 0.02$	$n = 0.03$	$n = 0.04$	$n = 0.05$	$n = 0.06$	$n = 0.07$	$n = 0.08$	$n = 0.09$	$n = 0.10$
20 m	90.99	80.6	74.2	67.32	63.69	60.82	58.54	56.44	54.73
30 m	89.23	79.8	72.79	67.01	63.65	60.87	58.54	56.66	54.84
40 m	88.64	78.89	71.49	67.07	63.7	60.92	58.67	56.65	54.92
50 m	86.52	77.56	71.75	67.39	64.07	61.15	58.78	56.82	55.2

Table 4. RMSE for different roughness values in each mesh resolution. The simulation with n $= 0.01$ for each resolution is used as the reference simulation. Unit is meter.

Maximum RMSE (m)	$n = 0.02$	$n = 0.03$	$n = 0.04$	$n = 0.05$	$n = 0.06$	$n = 0.07$	$n = 0.08$	$n = 0.09$	$n = 0.10$
20 m	0.0076	0.0114	0.014	0.0159	0.0174	0.0187	0.0197	0.0205	0.0212
30 m	0.0079	0.0119	0.0146	0.0166	0.0181	0.0192	0.0202	0.021	0.0218
40 m	0.0081	0.0122	0.015	0.0169	0.0184	0.0195	0.0205	0.0213	0.022
50 m	0.0083	0.0125	0.0152	0.0172	0.0187	0.0198	0.0208	0.0216	0.0223

4.5. Comparison with the observation

The model predictions were evaluated using observed data presented in figure 3. This is undertaken in two ways. First, the monitored flood-prone roads and reported flooded locations are compared with the model predictions to evaluate the general performance of the model simulation. Second, assuming that an event is reported immediately or shortly after it occurs by the public seeking for emergency support, we evaluate the dynamic performance of the model by considering the temporal dimension of the monitored/reported flood locations, and comparing this with the model predicted time series shown in figure 9.

The model predicted maximum inundated area is evaluated against the reported incident locations and roads where digital meters are installed in figure 12. Overall, 91.6% of the reported incidents fall within the predicted regions with a water depth greater than 2 cm, and 54.7% in the region of water depth greater than 5 cm. In particular, there is a good match between the predicted flooded areas and the clustering of incidents in the inner city districts (indicated with black circles). However, there is an overestimation of the inundated areas to the southeast of the river, and an underestimation to the northeast.

The point locations shown in figure 12 are segregated into different time periods based on the time that the incidents were reported. Figure 13 shows the number of reported incidents during the course of the day. This agrees well with the rainfall hyetograph (figure 2) in which the precipitation peaks at around 8:30 am. Incidents reported after 12:00 pm are likely to be residual incidents when rainfall has ceased.

The temporal distribution of the reported incidents is shown in figure 14, overlain with the maximum water depth reached till the corresponding time.

5. Discussion

5.1. Evaluating model sensitivity to mesh resolution and roughness specification

The evaluation of model sensitivity to mesh resolution reveals some interesting findings. Previous studies in fluvial flood modelling found diffusion-based (Yu and Lane 2006a) and inertial-based models (Ozdemir *et al* 2013) are rather sensitive to mesh resolution. From this set of simulations in this particular site, we can conclude that the model is relatively insensitive to mesh resolution (figure 4 and table 1) when the total inundated area is considered. There is a relatively minor difference in the peak inundation between the 20 m and 50 m simulations (<6%) for all roughness values. With the increase of roughness, the difference becomes more pronounced, for example, increasing from −0.2% to +3.3% for the 20 m simulations with an n value of 0.01 and 0.1, respectively. The overall

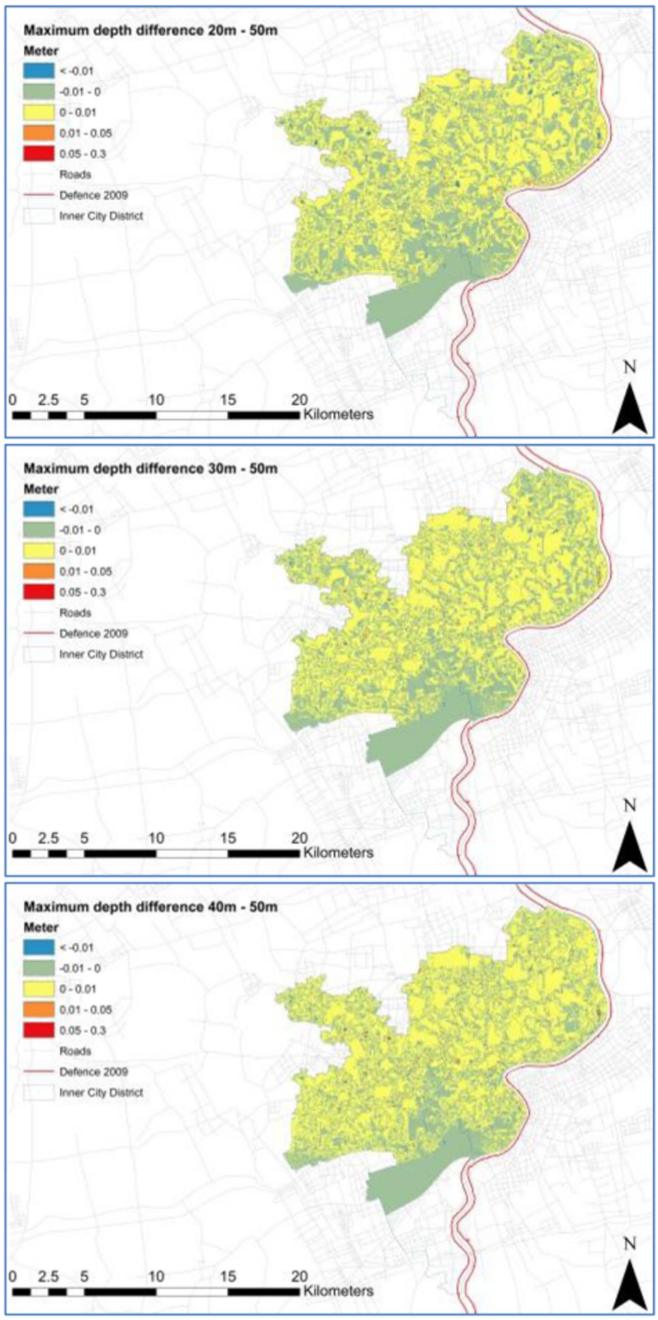

Figure 5. Difference in the maximum depth predicted by simulations with different mesh resolution.

difference in the predicted water depth over time is also notably minor (RMSE in figure 4(c) and table 4). However, when the spatial distribution of inundation is considered, the model becomes more sensitive to mesh resolution, evidenced by the Fit statistics shown in figure 4(b) and table 3. Table 3 also shows that, as the roughness value increases progressively, the spatial sensitivity diminishes. This is also reflected in the spatial distribution of maximum depth difference shown in figure 5, where the difference between the 50 m simulation and 40 m, 30 m and 20 m are compared.

In contrast, the model response is more sensitive to roughness specification compared to mesh resolution. In particular, the model response becomes increasingly sensitive to roughness with the coarsening of resolution (figure 4 and table 2). This is demonstrated by all three metrics. Comparing against the reference simulation of $n = 0.01$, the peak inundation difference of $n = 0.02$ and $n = 0.1$ increases from 2.1% to 11.7% for the 50 m simulation (table 2). The sensitivity is also demonstrated in the spatial agreement between the inundation extents obtained from simulations with different roughness values (figure 4(b) and table 3). Spatial difference of the predicted maximum water depths between the simulations with $n = 0.1$ and $n = 0.01$ for each mesh resolution shown in figure 6 suggests that, with a step

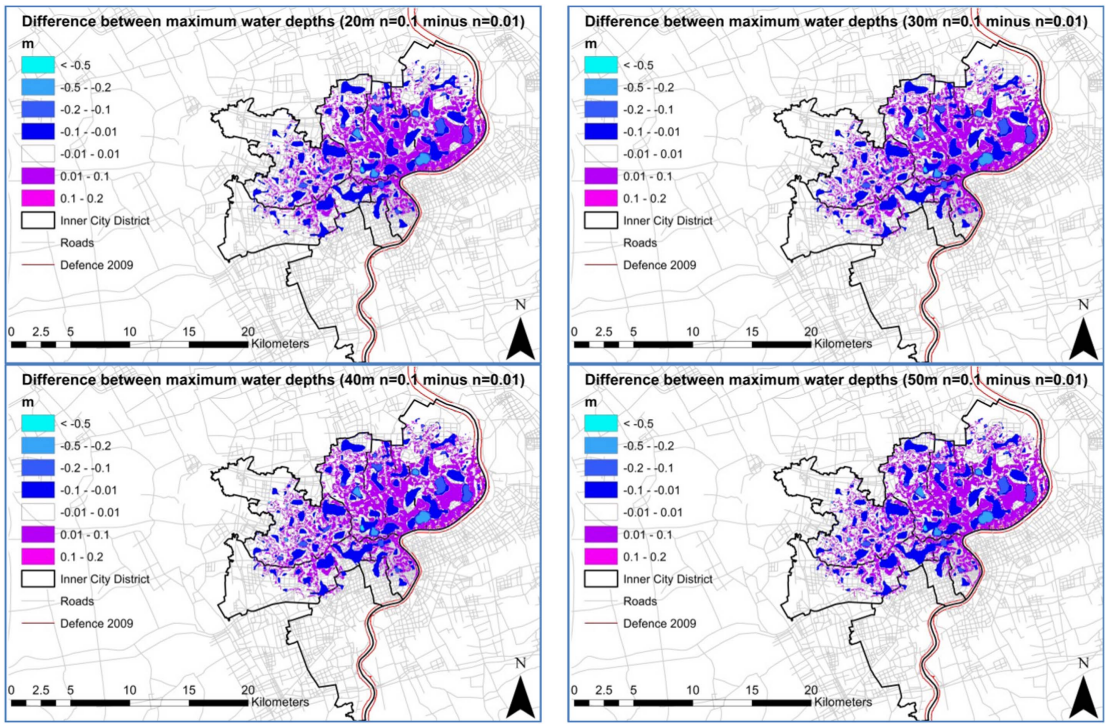

Figure 6. Difference in maximum water depth predicted by simulations with $n = 0.1$ and $n = 0.01$ for each mesh resolution.

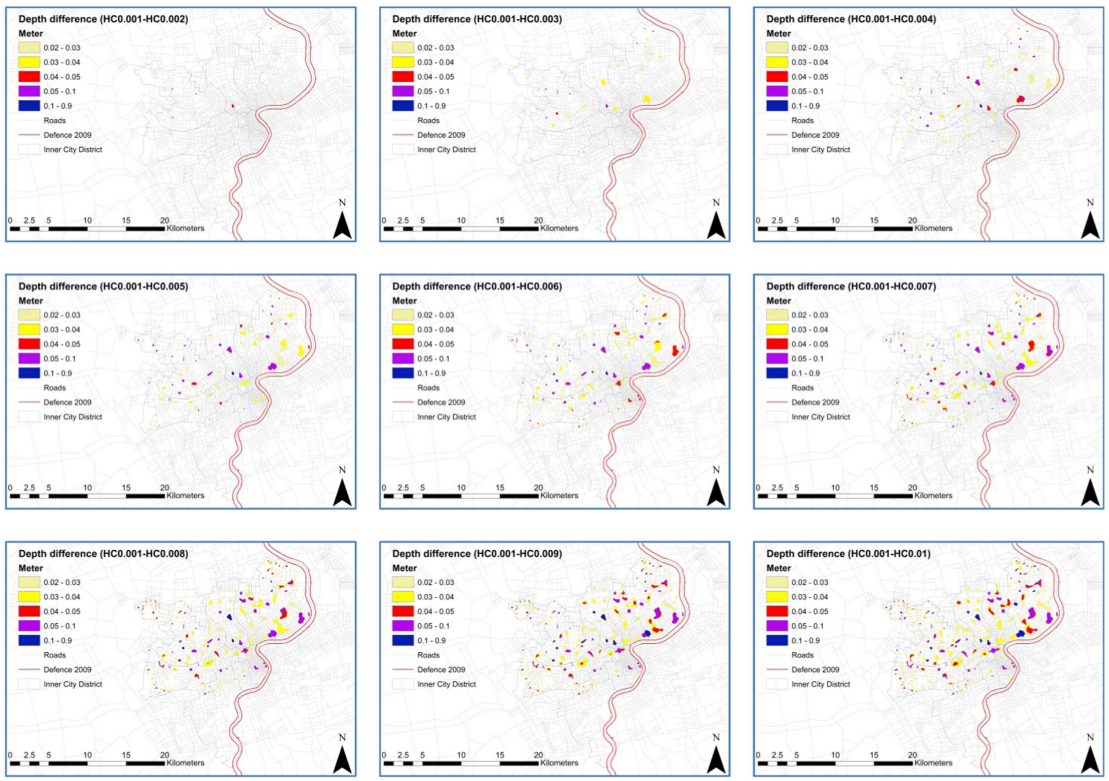

Figure 7. Difference in maximum water depth with different hydraulic conductivity (>2 cm).

increase of roughness value, there can be big difference between the maximum water depth predictions at the local level although globally the RMSE is small. For fluvial flood modelling, the net impact of increased roughness is slowed surface runoff locally. This, however, does not necessarily result in increased water depth locally. For hydro-inundation modelling, the response is more complex and depends on the local topography, rainfall intensity and parameters

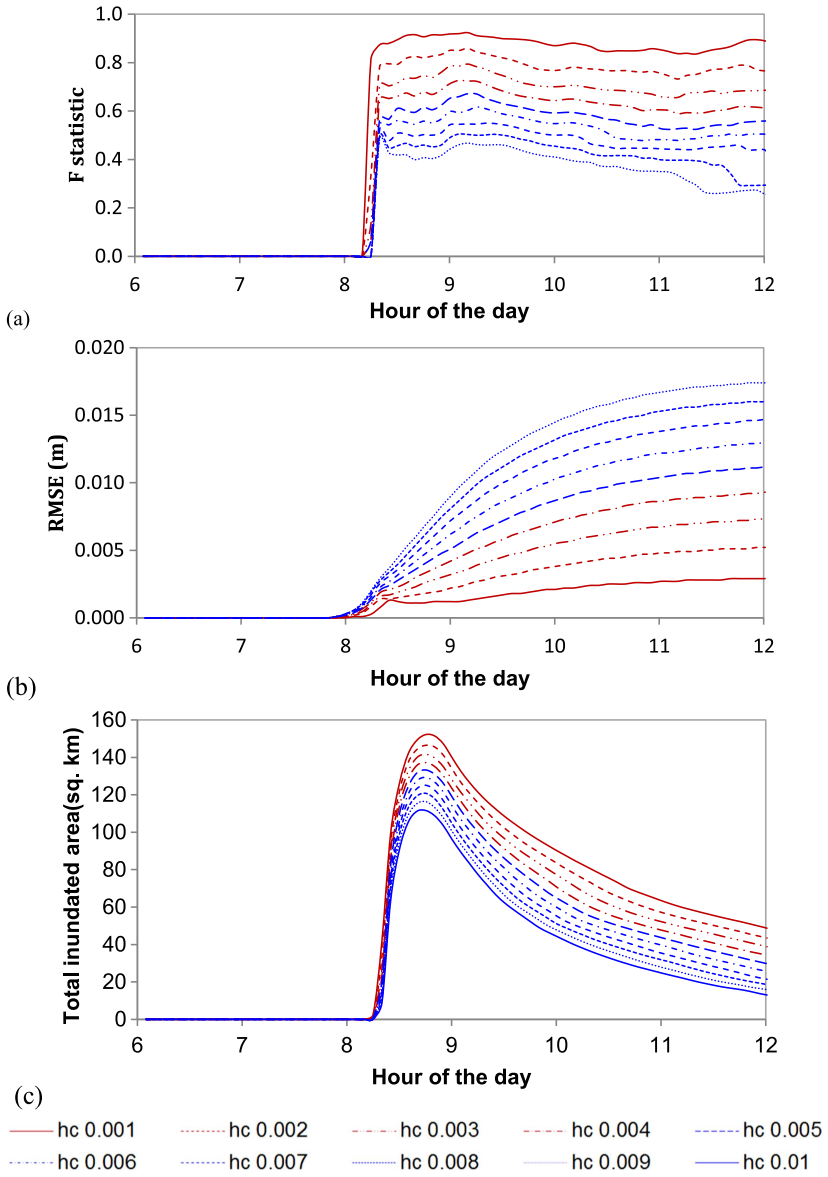

Figure 8. Sensitivity analysis to hydraulic conductivity. Figures show the comparison of (a) fit statistic, (b) root mean standard error and (c) total inundation area over time. For F and RMSE, the reference simulation is with a hydraulic conductivity value of 0.001 m hour^{-1}.

associated with infiltration, evapotranspiration and drainage.

Results demonstrate the complex interplay between mesh resolution and roughness specification for hydro-inundation modelling. With the consideration of hydrological processes, the surface flow routing suggests various degrees of model sensitivity to mesh resolution and floodplain roughness when evaluated against different metrics. Therefore, the model sensitivity is two-fold. On one hand, it is comparatively insensitive to varying mesh sizes, when the flood area is considered. On the other hand, the spatial metrics (i.e. F and RMSE) demonstrate greater spatio-temporal variability in the prediction than the global metric (i.e. total inundated area), suggesting that the model is relatively sensitive to mesh resolution and roughness specification.

5.2. Spatial and temporal evaluation of model prediction

Overall, given the spatial scale of prediction, the complexity involved in the urban topography and assumptions made in the modelling processing, the results are encouraging when considering the degree of agreement between the prediction and observation. The simplified model simulates the inundated areas reasonably well and reproduces areas that could have been flooded during the event with a good degree of predictive skill. The majority of the flooded areas are predicted to be within the inner city districts. This agrees well with the description of the event in the local media. In the inner city districts, surface flooding hotspots predicted by the model agrees well with the major clusters of crowd-sourced incidents (figure 12).

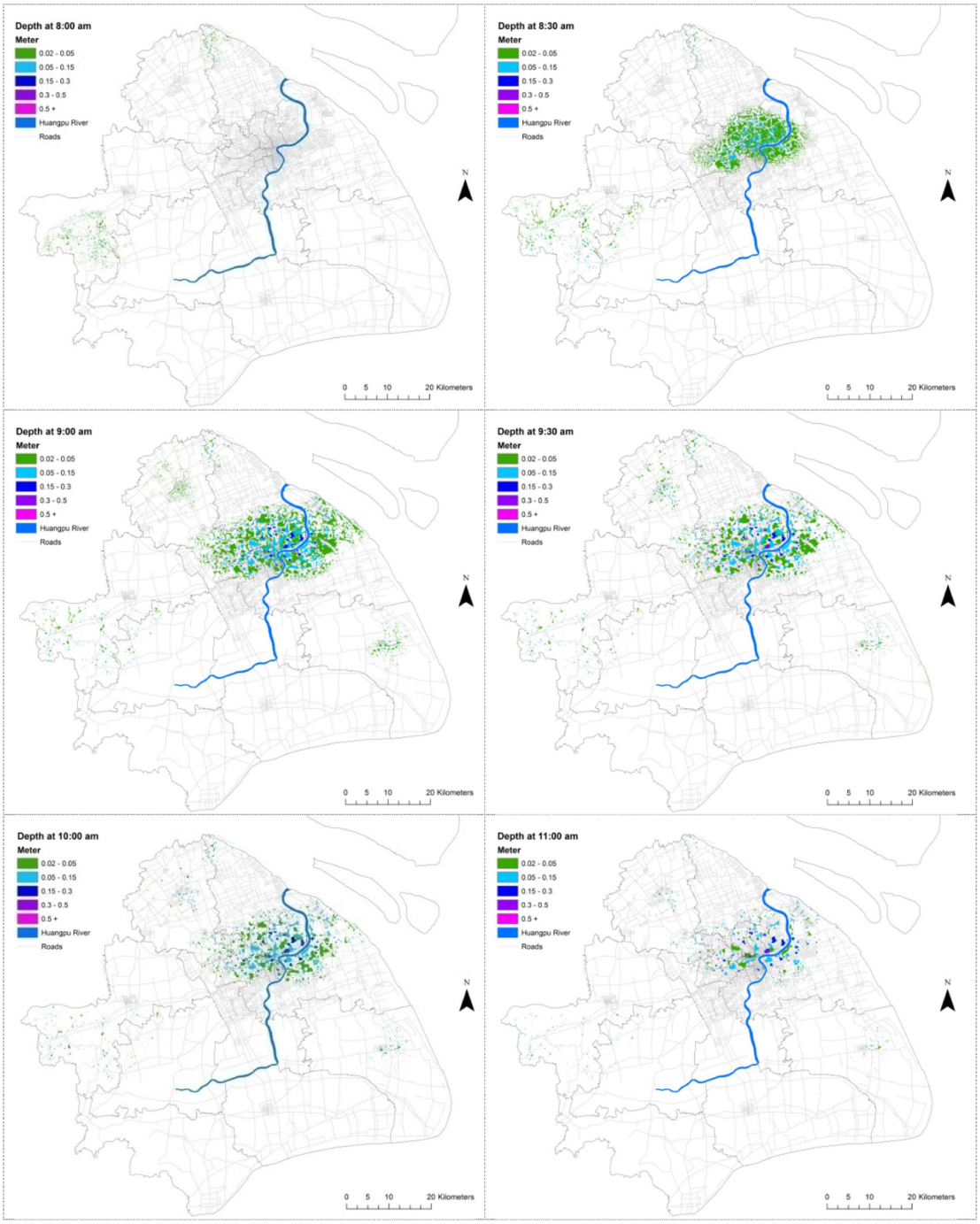

Figure 9. The predicted water depth greater than 2 cm during the storm.

Given the mild terrain of the inner city areas, surface water flooding tends to be locally-originated. Figure 15 shows the 0.5-meter contour lines plotted on top of the predicted flooded areas with a water depth of over 5 cm. This demonstrates that most of the worst hit areas are topographic lows, with ground elevation ranging between 2.5–4 meters. Reported incidents also tend to cluster in these areas.

An assessment of the temporal performance of the model is undertaken using reported incidents, assuming that an incident is reported shortly after it occurs. This is a reasonable assumption given the duration and magnitude of the storm event. Temporal comparison in figure 14 demonstrates the capacity of the model in predicting the dynamics of surface water flooding. In all the time periods considered, over 90% of the points are within the predicted water depth reached by the respective time point.

However, discrepancies between the model prediction and observation data are also noted. There are incidents reported in topographic highs where surface water flooding is not expected and vice versa. The discrepancies may arise from a number of sources, including the simplified nature of the model, quality of the input data and accuracy of the reported incidents. First, the model involves a number of structural

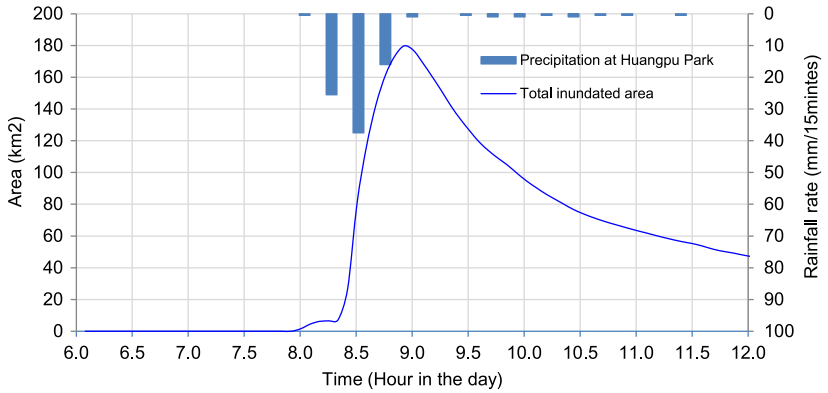

Figure 10. 15 min rainfall total in the Huangpu Park Station, and total inundation area (>2 cm) over time.

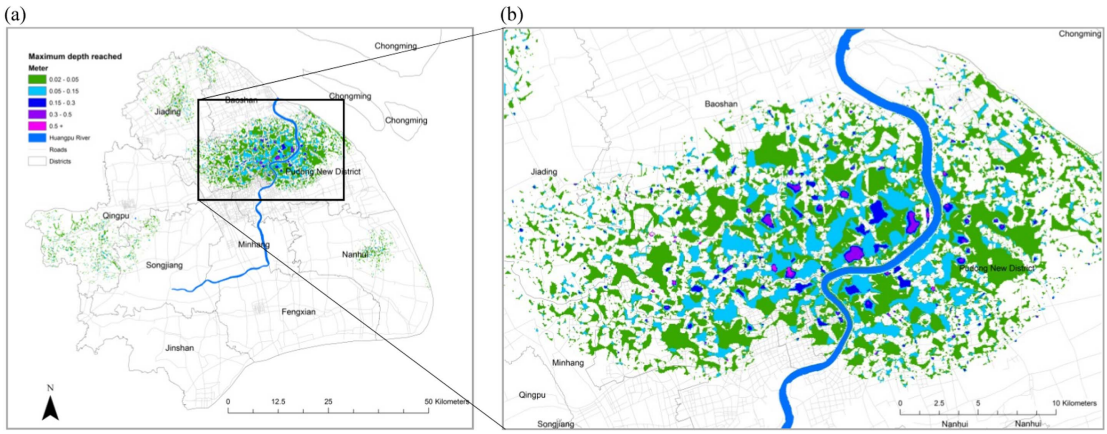

Figure 11. Maximum water depth predicted by the model: (a) at the city-scale; and (b) within the inner city districts.

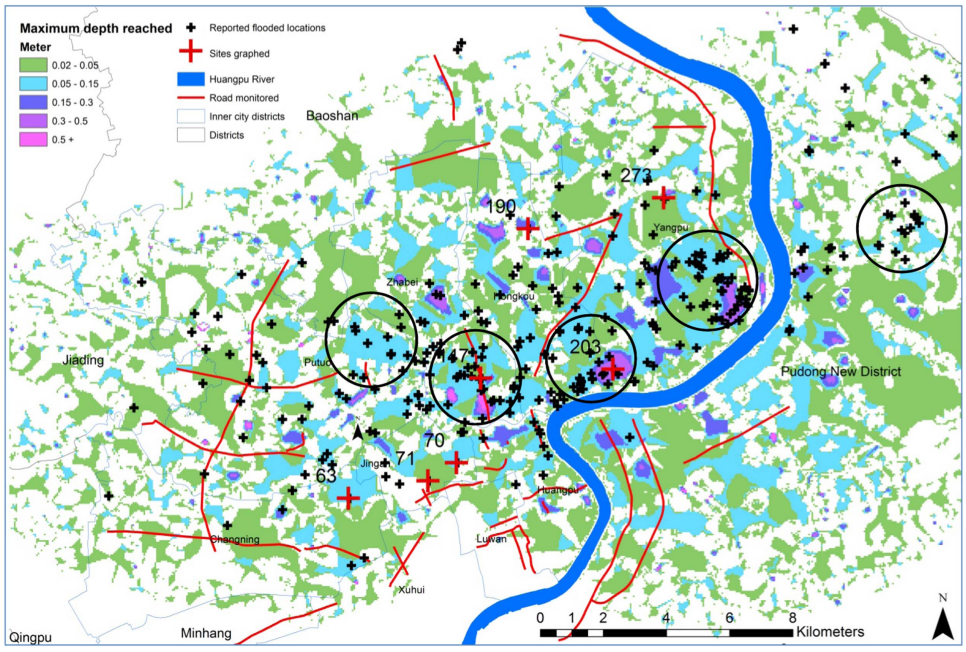

Figure 12. (i) Roads where monitoring points are located (red lines); and (ii) reported flooded locations; overlain with the predicted flood areas. Red crosses are the points where water depth and velocity are analyzed.

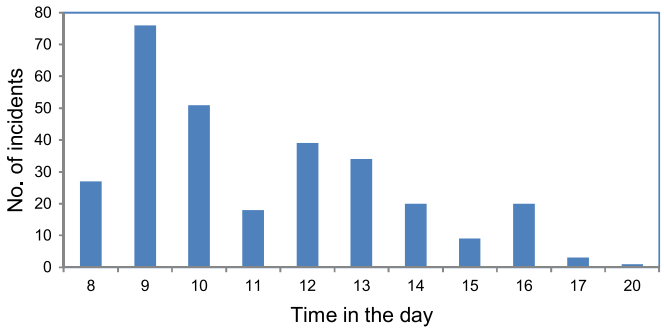

Figure 13. Number of incidents reported during the course of the day.

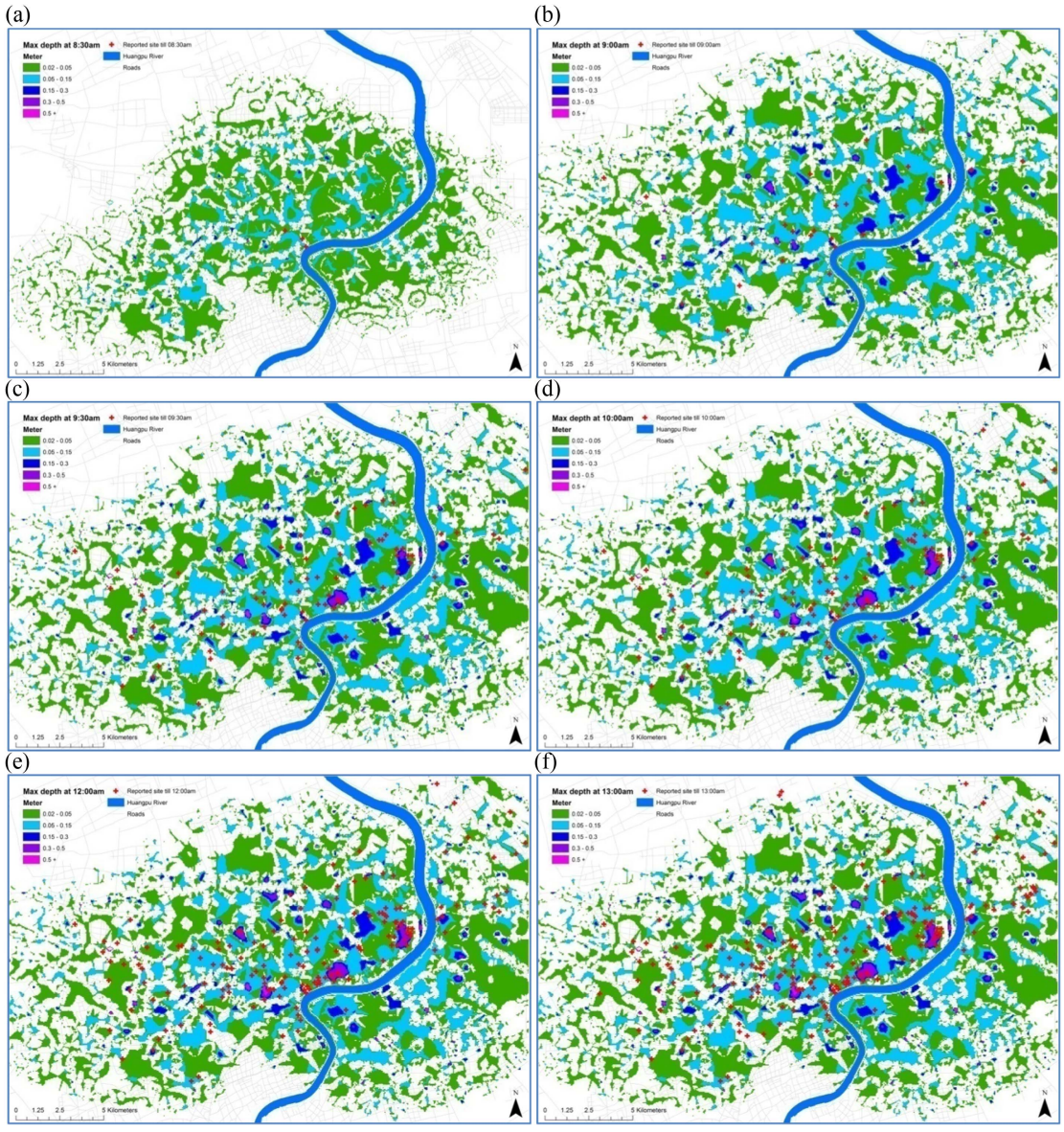

Figure 14. Spatial and temporal distribution of the reported incidents, overlain with the maximum water depth predicted till the time point. The percentage of points within the predicted inundation for (a)–(d) is 100%, 92.6%, 89.5%, 90.3, 91.3% and 91.5%, respectively.

assumptions. A major one is that surface runoff is the dominant source of flooding, thus surcharge is not considered. Due to the very mild terrain of Shanghai, sewer surcharge is known to be rare during flooding events, including the one simulated. However, in other environments, sewer surcharge may occur in

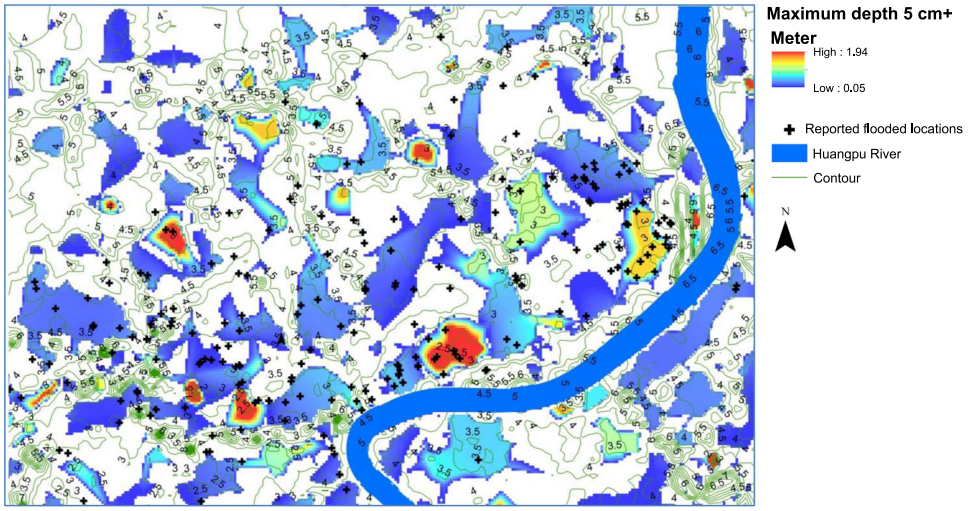

Figure 15. Predicted flooded areas and reported incident locations with the contour lines.

places where surface runoff is not present, or compound the effects of surface runoff. In such situations, underestimation is likely to occur and a dual drainage model should produce more robust results. Moreover, the model assumes a uniform mass loss for individual pixels to simply represent the drainage capacity. A similar method is used in Mignot *et al* (2006) used a similar method to treat the effect of storm sewer in an urban site. Distributed drainage capacity is used in the simulation. Although the bulk sum of the mass loss to storm sewers is expected to be reasonably well represented, the temporal capacity of the sewer system might be simplified as the interaction at the surface/sewer boundaries (manholes) has not been considered in the model. Due to the intensity of the storm event, it is expected that the drainage capacity has been reached early in the simulation. Therefore, the simulation might have overestimated the amount of mass loss to urban sewer system.

Second, the quality of the input data also contributes to the accuracy of the model predictions. Rainfall distribution is expected to be an important factor to consider. The relatively dense rain gauge network (44 stations) in Shanghai presents a good basis for the simulation. Given the degree of agreement between the predicted extent and observed data, the spatio-temporal distribution of precipitation appears to have been adequately represented by the gauging data, including the inner city. However, the discrepancies between model prediction and observation to the southeast of the Huangpu River (figure 12) are likely due to the poor quality of the rainfall data derived for the region. Model predicts a rather extensive area of flooding for the region. However, there are only a few reported incidents in this area. Precipitation might have been overestimated for the region during interpolation, where the gauging stations in the inner city are given more weighting due to their proximity to the site (figure 2). Therefore, the overall pattern of flooded areas might be correctly predicted but local predictions could be refined with a more accurate rainfall representation. Studies have investigated the effect of spatial pattern of precipitation on hydrological predictions (e.g. Obled *et al* 1994), including comparison with the use of weather radar (e.g. Cole and Moore 2008). Future research could be directed towards this area. Another source of input data uncertainty is related to the DEM. Urban topography can be complex due to the presence of manmade structures. This study used a 50 m DEM derived from a 0.5 m contour line dataset. Although the main topographic characteristics are expected to be represented in the dataset, local topographic complexities are unlikely to be adequately represented. The sub-grid treatment of DEM in city centre could be a solution to deal with this issue in future studies.

Third, there are inherent uncertainties in the reported incidents, in terms of the nature, timing and location. Most of the incidents have a house number or business address associated. However, street-level GIS maps with house numbers in Shanghai are not available to this study. The locations are determined based on the interpretation of Google Map service and geo-referenced in GIS. As a result, the locations of the incidents may contain errors. Similarly, the time when a site is flooded can be highly uncertain. This introduced uncertainty into the temporal evaluation. The number of incidents reported is also a factor to consider. We used 298 point incidents and segregated the points into a 30-minute and 1-hour interval. A larger number of points should allow a higher temporal resolution hence a more robust evaluation.

5.3. Evaluating hydraulic variables predicted

In addition to the inundated area, water depth and velocity are two variables that determine the magnitude of a surface water flood event, in particular at the local scale. The predictions of water depth and velocity

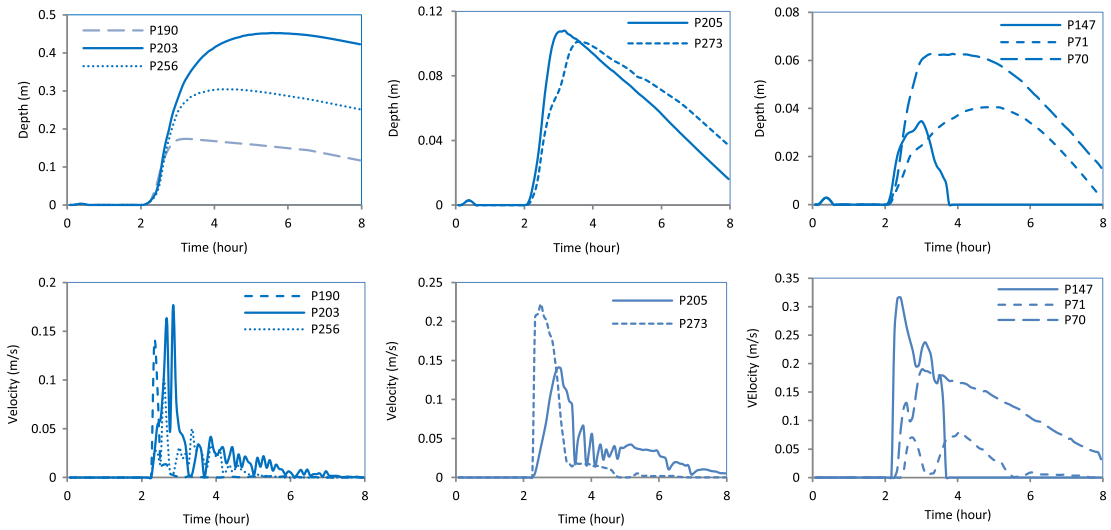

Figure 16. Time series of predicted water depth and velocity at 8 incident points (figure 8), with various peak water depths and velocity.

at 8 points where incidents were reported (figure 12) are shown in figure 16.

Time series of water depth and velocity for the 8 points demonstrate the capacity of the model in simulating hydraulic variables. Depth and velocity profiles capture the rising and recession phase of the flooding for individual points. Due to the local topographic configurations, the magnitude and pattern of the profiles differ from each other. Due to the lack of observation data, the model is not evaluated in this aspect. However, it is recognized that, although the general pattern of response is expected to agree with what happens in reality, the predictions of depth and velocity, in particular their timing, may not be sufficiently accurate due to the uncertainties in the input data and simplified nature of the model. The simulations are computationally stable in all cases. The variations noted in the velocity profiles are associated with surface flow runoff and often in synchronization with the intensity of rainfall.

6. Conclusion

The application of a simple surface water flood model for modelling city-scale surface water flood risks are described. Surface runoff, infiltration and evapotranspiration are the key processes represented in the model. The interaction between surface runoff and storm sewer systems is simplified. Drainage through storm sewers is treated as mass loss, linearly interpolated through time and assumed to be uniform over time for individual pixels but distributed across the simulation domain. The application demonstrates the capacity of the model for deriving the broad areas vulnerable to surface water flood risks at the city-scale, and during extreme flood events when surface runoff is significant compared to sewer surcharge.

The model was applied to hindcast surface water flooding during an extreme storm event occurred in Shanghai on 12 August 2011. Results are compared with the spatial and temporal distribution of the incidents reported by the public through a web-based emergency system. A good degree of agreement is reached and over 91.6% of the reported incidents fall within the predicted inundated areas (2 cm+). A preliminary assessment of the model's dynamic performance using the temporal information in the crowdsourced data also demonstrates a good level of agreement. However, limiting the analysis to a single historical flood event can be restrictive, a larger number of pluvial flood cases could be analyzed to arrive at more robust conclusions.

One key advantage of the model is the minimum requirements for the information regarding the storm sewer systems, the role of which is simplified using a bulk value that represents the drainage capacity at difference areas. This is particularly advantageous for the city-scale study where subsurface storm sewer data might not be available. On the other hand, the accuracy of distributed rainfall and urban topography are the two key datasets that influence model predictions. The model application demonstrates that, with a reasonable coverage of rainfall data and an adequate representation of urban topography, a good level of prediction can be reached.

While water depth is not the predictive focus for the application, a refinement of the model and the use of more robust data should allow improved predictions of distributed water depth. In terms of floodplain topography, buildings are not represented in the DEM used in this study. However, given the scale and focus of the modelling, this is considered to be adequate. Theoretically, the model could be applied at a local scale with a finer resolution. However, at a local scale, if the focus is detailed prediction of hydraulic

variables, a finer topography that directly represents buildings adequately is required and the effect of building representation has been investigated for fluvial flood modelling (Schubert and Sanders 2012). Alternatively, literature has seen approaches to represent buildings in coarse mesh resolution using the multi-layer approach (e.g. Chen *et al* 2012). Therefore, further studies could be undertaken to evaluate whether the model can be used to reproduce the spatial and temporal variation of water depths, at a local scale and with the representation of buildings.

The validation of predicted flow variables for surface water flooding is a challenging area of research due to its sudden and fast-developing nature. Therefore, validation data is often obtained on an opportunistic basis. Recent research has seen novel approaches to the derivation of flow variables, including the use of video recordings to estimate velocity and water depth (Aronica *et al* 2014). Advances in remote sensing technology may also provide validation data in near future.

The predictions obtained with the simplified modelling approach could be useful to decision makers as a first-stage evaluation of the places potentially vulnerable to surface water flood risks at the city-scale. If combined with rainfall forecasting (e.g. Quantitative Precipitation Forecast), the model presented here could provide a preliminary city-wide flood inundation prediction which can help for emergency response and warning. A scenario-based approach could be undertaken to evaluate potential risks under a range of precipitation, drainage improvement and urban development scenarios. Subsequent work could be conducted in the vulnerable locations (e.g. north part of the city centre) to guide robust adaptation measures (structural or non-structural measures), assisted by more detailed hydraulic modelling (e.g. the dual drainage approach), considering the role of storm sewer systems. Results can also be used to assess vulnerabilities of the city to surface flooding in terms of its critical infrastructure, including, e.g., transport, communication and energy supply network/nodes (e.g. sub-stations) under a changing climate.

Acknowledgments

This research was supported by the National Natural Science Foundation of China (Grant No: 41201550, 41371493) and the Project of Joint Center for Shanghai Meteorological Science and Technology (Grant No: 2015-03). We thank the reviewers for their very useful and constructive comments.

References

Aronica G T, Cavalli M, Gaume E, Marchi L, Naso S and Borga M 2014 Post flash flood field investigations and analysis: the event of 22 November 2011 in the Longano catchment, Italy *European GeoSciences Union General Assembly* vol 16, EGU2014-15534

Aronica G T and Lanza L G 2005 Drainage efficiency in urban areas: a case study *Hydrol. Process.* **19** 1105–19

Bates P D and De Roo A P J 2000 A simple raster-based model for flood inundation simulation *J. Hydrol.* **236** 54–77

Bates P D, Horritt M and Fewtrell T 2010 A simple inertial formulation of the shallow water equations for efficient two-dimensional flood inundation modelling *J. Hydrol.* **387** 33–45

Calder I R, Harding R J and Rosier P T W 1983 An objective assessment of soil moisture deficit models *J. Hydrol.* **60** 329–55

Chen A S, Evans B, Djordjević S and Savić D A 2012 Multi-layered coarse grid modelling in 2D urban flood simulations *J. Hydrol.* **470** 1–11

Chin J 2012 Deadly Beijing floods spark anger, prompt infrastructure questions *The Wall Street Journal* (Accessed: 7 January 2014)

Cole S J and Moore R J 2008 Hydrological modelling using raingauge- and radar-based estimators of areal rainfall *J. Hydrol.* **358** 159–81

DHI. 2010 *MIKE 21. Flow Model Hydrodynamic Module Scientific Documentation* (Hørsholm, Denmark: DHI)

Djordjević S, Ivetić M, Maksimović C and Rajcević A 1991 An approach to the simulation of street flooding in the modeling of surcharged flow in storm sewers *Proceedings: New Technologies in Urban Drainage* ed U D T Maksimovic (Amsterdam: Elsevier) pp 101–8

Dong Z Y and Lu J R 2008 Numerical simulation of urban waterlogging disaster due to plum storm *Proc. of 16th IAHR-APD Congress and 3rd Symp. of IAHR-ISHS* (Nanjing: Hohai University Press)

Fewtrell T J, Duncan A, Sampson C, Neal J C and Bates P D 2011 Benchmarking urban flood models of varying complexity and scale using high resolution terrestrial LiDAR data *Phys. Chem. Earth* **36** 281–91

Hamill L 2010 *Understanding Hydraulics* 3rd edn (Basingstoke: Palgrave and Macmillan) pp 631

Hénonin J, Ma H, Yang Z Y, Hartnack J, Havnø K, Gourbesville P and Mark O 2013 Citywide multi-grid urban flood modelling: the July 2012 flood in Beijing *Urban Water Journal* (doi:10.1080/1573062X.2013.851710)

Horritt M S and Bates P D 2001 Effects of spatial resolution on a raster based model of flood flow *J. Hydrol.* **253** 239–49

Hsu M H, Chen S H and Chang T J 2000 Inundation simulation for urban drainage basin with storm sewer system *J. Hydrol.* **234** 21–37

IPCC 2007 *Climate Change 2007: The Scientific Basis* (Cambridge: Cambridge University Press)

Leandro J, Chen A S, Djordjević S and Savić D 2009 Comparison of 1D/1D and 1D/2D coupled (sewer/surface) hydraulic models for urban flood simulation *J. Hydraulic Eng.* **135** 495–504

Mark O, Weesakul S, Apirumanekul C, Aroonnet S B and Djordjević S 2004 Potential and limitations of 1D modelling of urban flooding *J. Hydrol.* **299** 284–99

Maksimović C, Prodanović D, Boonya-Aroonnet S, João, Leitão P, Djordjević S and Allitt R 2009 Overland flow and pathway analysis for modelling of urban surface water flooding *J. Hydraul. Res.* **47** 512–23

Mignot E, Paquier A and Haider S 2006 Modeling floods in a dense urban area using 2D shallow water equations *J. Hydrol.* **327** 186–99

Obled C, Wendling J and Beven K 1994 The sensitivity of hydrological models to spatial rainfall patterns: an evaluation using observed data *J. Hydrol.* **159** 305–33

Ochoa-Rodriguez S *et al* 2015 Impact of spatial and temporal resolution of rainfall inputs on urban hydrodynamic modeling: a multi-catchment investigation *J. Hydrol.* **531** 389–407

Oosterbaan R J and Nijland H J 1994 ed H P Ritzema *Drainage Principles and Applications. International Institute for Land Reclamation and Improvement (ILRI)* Publication 16, second revised edition, 1994 (The Netherlands: Wageningen)

Ozdemir H, Sampson C, de Almeida, Gustavo A M and Bates P D 2013 Evaluating scale and roughness effects in urban flood modelling using terrestrial LIDAR data *Hydrol. Earth Syst. Sci.* **10** 5903–42

Pitt M 2008 *Learning Lessons from the 2007 Floods (The Pitt Review)* Final report, June 2008 (London: Cabinet Office) (http://archive.cabinetoffice.gov.uk/pittreview/thepittreview/final_report.html)

Sampson C, Bates P B, Neal J C and Horritt M S 2013 An automated routing methodology to enable direct rainfall in high resolution shallow water models *Hydrol. Process.* **27** 467–76

Schmitt T G, Thomas M and Ettrich N 2004 Analysis and modelling of flooding in urban drainage systems *J. Hydrol.* **299** 300–11

Schubert J E and Sanders B F 2012 Building treatments for urban flood inundation models and implications for predictive skill and modelling efficiency *Adv. Water Resour.* **41** 49–64

Seyoum S D, Vojinovic Z, Price R K and Weesakul S 2012 Coupled 1D and Noninertia 2D Flood Inundation Model for Simulation of Urban Flooding *J. Hydraulic Eng.* **138** 23–4

Smedema L K and Rycroft D W 1983 *Land drainage: planning and design of Agricultural Drainage Systems* (London: Batsford)

Smith M 2006 Comment on 'Potential and limitations of 1D modeling of urban flooding' by O Mark *et al* [J Hydrol 299 (2004) 284–299] *J. Hydrol.* **321** 1–4

St Domingo N D, Refsgaard A, Mark O and Paludan B 2010 Flood analysis in mixed-urban areas reflecting interactions with the complete water cycle through coupled hydrologic-hydraulic modelling *Water Science & Technology* **62** 1386–92

Wang L P, Ochoa-Rodriguez S, Onof C and Willems P 2015 Singularity-sensitive gauge-based radar rainfall adjustment methods for urban hydrological applications *Hydrol. Earth Syst. Sci.* **19** 4001–21

Wu X, Yu D, Wilby R L and Chen Z 2012 An evaluation of the impacts of land surface modification, storm sewer development, and rainfall variation on waterlogging risk in Shanghai *Nat. Hazards* **63** 305–23

Xu N 2012 *Beijing Floods: not Enough Prevention. The Guardian* (Accessed: 7 January 2014)

Yin J, Yu D, Yin Z E, Wang J and Xu S Y 2013a Multiple scenario analyses of Huangpu River flooding using a 1D/2D coupled flood inundation model *Nat. Hazards* **66** 577–89

Yin J, Yu D, Yin Z E, Wang J and Xu S Y 2013b Modelling the combined impacts of sea-level rise and land subsidence on storm tides induced flooding of the Huangpu River in Shanghai, China *Clim. Change* **119** 919–32

Yin J, Yu D and Wilby R 2016a Modelling the impact of land subsidence on urban pluvial flooding: A case study of downtown Shanghai, China *Sci. Total Environ.* **544** 744–53

Yin J, Yu D, Yin Z, Liu M and He Q 2016b Evaluating the impact and risk of pluvial flash flood on intra-urban road net-work: A case study in the city centre of Shanghai, China *J. Hydrol.* **537** 138–45

Yu D and Coulthard T J 2015 Evaluating the importance of catchment hydrological parameters for urban surface water flood modelling using a simple hydro-inundation model *J. Hydrol.* **524** 385–400

Yu D and Lane S N 2006a Urban fluvial flood modelling using a two-dimensional diffusion wave treatment, part 1: mesh resolution effects *Hydrol. Process.* **20** 1541–65

Yu D and Lane S N 2006b Urban fluvial flood modelling using a two-dimensional diffusion wave treatment, part 2: development of a sub grid-scale treatment *Hydrol. Process.* **20** 1567–83

Yu D and Lane S N 2011 Interaction between subgrid-scale resolution, feature representation and grid-scale resolution in flood inundation modelling *Hydrol. Process.* **25** 36–53

Yuan Z L 1999 *Flood and Drought Disasters in Shanghai* (Nanjing: Hohai University Press) (in Chinese)

Zhai P M, Zhang W B, Wan H and Pan X H 2005 Trends in total precipitation and frequency of daily precipitation extremes over China *J. Clim.* **18** 1096–108